scientific reports

Check for updates

OPEN

Adapalene, an RAR agonist, exerts anti-inflammatory effects by regulating macrophage polarization through RARβ -mediated signaling pathways

Na Hyun Lee[1], Mi Jin Choi[2], Seong Mi Ji[2], Hyun Jeong Kwak[3]✉ & Hyae Gyeong Cheon[1,2]✉

Retinoic acid receptor (RAR) is a nuclear receptor that plays a critical role in regulating cellular proliferation and differentiation through transcriptional control. However, its role in the macrophage inflammatory response remains poorly understood. In the present study, we explored the effects of adapalene, a selective RARβ and RARγ agonist, on lipopolysaccharide (LPS)-induced inflammation in RAW264.7 cells. Adapalene inhibited the LPS-induced inflammatory response in a concentration-dependent manner, whereas the anti-inflammatory effects of adapalene were attenuated by RARβ-targeting small interfering RNA (siRNA) or an RARβ antagonist (LE135). Mechanistic investigations revealed that adapalene suppressed LPS-induced phosphorylation of the MAPK and PI3K/Akt pathways, thereby inhibiting the nuclear translocation of NF-κB in RAW264.7 cells. In addition, adapalene upregulated the expression of anti-inflammatory M2 macrophage markers, accompanied by increased STAT3 phosphorylation. The acute administration of adapalene to C57BL/6J mice protected against LPS-induced inflammation, liver damage, and septic shock-related mortality in vivo. Furthermore, chronic oral administration of adapalene in high-fat diet (HFD)-induced obese mice reduced pro-inflammatory markers while increasing anti-inflammatory markers in the liver. These findings suggest that adapalene exerts potent anti-inflammatory effects in macrophages through RARβ activation, thus highlighting its potential as a therapeutic agent for treating inflammatory and metabolic disorders.

Keywords Adapalene, Retinoic acid receptor, Inflammation, Lipopolysaccharide, Macrophage

Macrophages play a central role in recognizing and clearing invading pathogens, while regulating various physiological and pathological processes, including inflammation, systemic metabolism, tissue homeostasis, and angiogenesis[1,2]. Notably, they contribute to both innate and adaptive immunity and serve as regulators and effector cells in humoral and cell-mediated immune responses[3]. Macrophage populations are heterogeneous and broadly categorized into the classical pro-inflammatory M1 phenotype and alternative anti-inflammatory M2 phenotype. These phenotypes can dynamically undergo transition between each other in response to different stimuli[4]. Notably, shifts in macrophage subpopulations within white adipose tissues play a significant role in metabolic diseases. For instance, in obese animal models, M1 macrophages infiltrate adipose tissue, leading to low-grade chronic inflammation and insulin resistance[5,6]. Conversely, M2 macrophages help to suppress obesity-induced inflammation, indicating their potential therapeutic implications for metabolic disorders[7,8]. Various transcription factors, including STAT, C/EBPβ, KLF, AP-1, NF-κB, and PPARs, have been identified as key regulators of the M1-to-M2 switch[2,9].

Retinoic acid receptors (RARs) are a group of nuclear receptors that function as transcription factors to regulate gene expression. They form heterodimers with the retinoid X receptor (RXR) and bind to retinoic acid response elements (RAREs) within the promoter regions of target genes[10]. The RAR family comprises RARα,

[1]Department of Health Sciences and Technology, GAIHST, Incheon, Republic of Korea. [2]Department of Pharmacology, College of Medicine, Gachon University, Incheon, Republic of Korea. [3]Department of Bio and Fermentation Convergence Technology, Kookmin University, Seoul, Republic of Korea. ✉email: hjkwak@kookmin.ac.kr; hgcheon@gachon.ac.kr

RARβ, and RARγ. While RARα is ubiquitously expressed, RARβ and RARγ exhibit tissue-specific expression patterns. They are involved in various biological processes, including embryonic development, homeostasis, cell proliferation, differentiation, and death[11,12]. Numerous studies have highlighted the role of RARs in modulating immune cell function by reducing the expression of inducible nitric oxide synthase (iNOS), pro-inflammatory cytokines, chemokines, and prostaglandins[13]; however, the specific subtypes involved in these actions remain unidentified. All-trans retinoic acid (ATRA), the endogenous ligand for all RAR subtypes (RARα, RARβ, and RARγ), functions at nanomolar concentrations[14]. ATRA has been proposed as an anti-inflammatory therapy that modulates M1 and M2 macrophage polarization[15–17]. Additionally, ATRA directly inhibits the production of pro-inflammatory cytokines in activated monocytes and macrophages[18,19].

Although ATRA has shown promising anti-inflammatory effects in rodent models through various mechanisms, it is associated with serious side effects[20]. This has led to the development of selective synthetic RAR ligands as potential therapeutic agents for the treatment of inflammation and related metabolic disorders.

Adapalene, a third-generation retinoid, is widely used as a first-line treatment for acne vulgaris due to its high affinity for RARβ and RARγ receptors (Kd = 34 and 130 nM, respectively), while exhibiting significantly lower activity on RARα (Kd = 1100 nM)[21]. To evaluate the potential of adapalene as an anti-inflammatory drug and uncover its mechanisms of action, we examined its effects on lipopolysaccharide (LPS)-induced inflammation in murine macrophages (RAW264.7), an in vivo LPS-induced septic shock model, and a high-fat diet (HFD)-induced obese model.

Materials and methods

Reagents

High-glucose Dulbecco's modified Eagle's medium (DMEM), fetal bovine serum (FBS), penicillin, and streptomycin were purchased from Gibco Inc. (Grand Island, NY, USA). Monoclonal antibodies against β-actin, Histone3, ERK, p-ERK (Tyr204), JNK, p-JNK (Thr183/Tyr185), p38 MAPK, p-p38 MAPK (Thr180/Tyr182), TNFα, COX-2, RARα, RARβ, RARγ and Arg1, polyclonal antibodies against iNOS, p65, and RARβ small interfering RNA (siRNA) were from Santa Cruz Biotechnology, Inc. (Delaware, CA, USA). Monoclonal antibodies against p-Akt (Thr309), p-PI3K (Tyr508), p-IκBα (Ser32), and STAT3, and polyclonal antibodies against PI3K, p-STAT3 (Tyr705) and p-p65 (Ser536) were purchased from Cell Signaling Technology Inc. (Danvers, MA, USA). Polyclonal antibodies against Akt, IL-1β, IL-6 and IκBα were from Abcam, Inc. (Cambridge, UK). Polyclonal antibodies against MRC1 were purchased from Bioworld Technology (Minneapolis, MN, USA). The M-MLV reverse transcriptase and random oligonucleotide primers were purchased from Promega (Madison, WI, USA). TOP script™ RT Dry MIX was obtained from Enzynomics Co. Ltd. (Daejeon, Korea). The Thunderbird SYBR qPCR mix was purchased from TOYOBO Co., Ltd. (Osaka, Japan). GAPDH, TNFα, IL-1β, IL-6, iNOS, COX-2, MRC1, Arg1, and RARβ oligonucleotide primers were from Bioneer (Daejeon, Korea). Lipofectamine RNA iMAX reagent was purchased from Invitrogen (Carlsbad, CA, USA). Enzyme-linked immunosorbent assay (ELISA) kits for PGE2, TNFα, IL-6, and IL-1β were from R&D Systems (Minneapolis, MN, USA). Adapalene, LE135, LPS, and other chemicals were purchased from Sigma-Aldrich (St. Louis, MO, USA).

Cell culture

Murine macrophages (RAW264.7; Korean Cell Line Bank, Seoul, Korea) were cultured at 37 ℃ in DMEM supplemented with 10% heat-inactivated FBS, 1% penicillin and streptomycin (100 U/mL) in a humidified 5% CO_2 atmosphere, and seeded in 6-well plate at a density of 3×10^6 cells/well. Cells were pretreated with adapalene (10, 100, or 1000 nM) before stimulation with LPS (100 ng/mL) for the indicated time periods. The adapalene concentrations were selected based on preliminary concentration–response experiments and previously published studies[22].

Real-time reverse transcription-polymerase chain reaction (RT-PCR)

Total RNA was extracted from macrophages using the Easy Blue Kit (Intron Biotechnology, Seongnam, Korea). TOP script™ RT Dry MIX and Oligo dT primers were used to synthesize cDNA from RNA. The sequences of primer used were as follows: GAPDH *(NM_008084.3)* forward, 5'-AGG TCG GTG TGA ACG GAT TTG-3' and reverse, 5'-GGG GTC GTT GAT GGC AAC A-3'; TNFα *(NM_013693.3)* forward, 5'-ATG GTC AGT AGA CTT TTA CA-3' and reverse, 5'-ATG AGC ACA GAA AGC ATG ATC-3'; IL-1β *(NM_008361.4)* forward, 5'- GCA ACT GTT CCT GAA CTC AA-3' and reverse, 5'- ATC TTT TGG GGT CCG TCA AC-3'; IL-6 *(NM_031168.2)* forward, 5'- GAG GAT ACC ACT CCC AAC AG-3' and reverse, 5'- AAG TGC ATC ATC GTT GTT CA-3'; iNOS *(NM_010927.4)* forward, 5'- GGA GTG ACG GCA AAC ATG AC-3' and reverse, 5'- TCG ATG CAC AAC TGG GTG AA-3'; COX-2 *(NM_011198.5)* forward, 5'-AAG ACT TGC CAG GCT GAA CT -3' and reverse, 5'-CTT CTG CAG TCC AGG TTC AA -3'; MRC1 *(NM_008625.2)* forward, 5'-GAG AGC CAA GCC ATG AGA AC -3' and reverse, 5'-GTC TGC ACC CTC CGG TAC TA-3'; Arg1 *(NM_007482.3)* forward, 5'-CAT GGG CAA CCT GTG TCC TT-3' and reverse, 5'-CGA TGT CTT TGG CAG ATA TGC A-3'; RARα *(NM_009024.2)* forward, 5'- AGA CAA GGT GGA CAT GCT GCA AGA-3' and reverse, 5'- TGA TGC TCC GAA GGT CTG TGA TCT-3'; RARβ *(NM_011243.3)* forward, 5'-AGA TGA CAG CGG AGC TAG AC-3' and reverse, 5'-TTC GTG GTG TAT TTA CCC AG-3'; RARγ *(NM_011244.5)* forward, 5'-GAC AGC TAT GAA CTG AGT CC-3' and reverse, 5'-CCT TAC AGA CCT CGT CT-3'.

Western blot analysis

The treated cells or liver tissues were washed twice with phosphate-buffered saline (PBS) and lysed using PRO-PREP protein extraction buffer (Intron Biotechnology) containing a protease and phosphatase inhibitor cocktail. The lysates were incubated on ice for 30 min and then centrifuged at 20,000 × g for 30 min at 4 ℃. Protein concentrations were determined using a protein assay reagent (Bio-Rad). For each sample, 30 μg of protein was

subjected to 8–10% sodium dodecyl sulfate (SDS)-polyacrylamide gel electrophoresis (PAGE) and transferred to polyvinylidene fluoride membranes. After transfer, membranes were cut horizontally according to the expected molecular weights of target proteins prior to antibody incubation to allow probing of multiple targets. The membranes were blocked with 4% skim milk in Tris-buffered saline containing 0.1% Tween 20 (TBS-T) for 1 h at room temperature. They were then incubated overnight at 4 ℃ with the primary antibody (1:1000) in 2% bovine serum albumin (BSA; MP Biomedicals, Santa Ana, CA, USA). After washing the membranes thrice with TBS-T for 10 min each, they were incubated with a horseradish peroxidase (HRP)-conjugated secondary antibody (1:5000) (Bioworld Technology) for 1.5 h at room temperature. Membranes were washed five times with TBS-T and developed using enhanced chemiluminescence (Millipore, Burlington, MA, USA). All protein levels were normalized to β-actin. All available blot images corresponding to the experiments reported in this study are provided in the Supplementary Information.

RAR siRNA transfection

RAW264.7 cells (3×10^6 cells/well in a six-well plate) were transfected with mouse RARβ siRNA or control siRNA using serum free DMEM containing a complex of Lipofectamine™ RNA iMAX reagent. RNA iMAX and siRNA were diluted in serum-free medium, incubated for 5 min, and mixed for 25 min. After transfection with 100 nM RARβ siRNA for 6 h, the cells were incubated in DMEM supplemented with heat-inactivated 10% FBS, penicillin, and streptomycin sulfate (100 mg/mL) for 18 h.

Fluorescence-activated cell sorting (FACS) analysis

RAW264.7 cells (1×10^6 cells/well in a six-well plate) were pre-treated with adapalene (10, 100, or 1000 nM) for 18 h, followed by stimulation with LPS (100 ng/mL) for 6 h. The cells were washed thrice with PBS and resuspended in FACS buffer. For flow cytometry, the cells were blocked with TruStain fcX™ (anti-mouse CD16/32 antibody; BioLegend, San Diego, CA, USA) for 15 min on ice. The cells were then incubated with fluorescent-labeled antibodies for 30 min on ice in the dark and washed again with FACS buffer. Antibodies were used for identification of RAW264.7 cells: fluorescein (FITC)-conjugated anti-mouse F4/80 (BioLegend, #123107), FITC-conjugated IgG2a rat isotype control, APC-conjugated anti-mouse CD86 (BioLegend, #123110) as the M1 marker, APC-conjugated anti-mouse CD206 (BioLegend, #141708) as the M2 marker, and APC-conjugated IgG2a rat isotype control. The cells were analyzed using a BD FACSCalibur™ flow cytometer (BD Biosciences). A minimum of 10,000 cells per sample were acquired and analyzed using FlowJo software. Gating thresholds were

1 st Antibody	Manufacturer	Cat. no	Host species	Dilution
TNFα	Cell Signaling	3707	Mouse	1:1000
IL-1β	Abcam	ab9722	Rabbit	1:1000
IL-6	Abcam	ab6672	Rabbit	1:1000
iNOS	Santa Cruz	sc-651	Rabbit	1:500
COX-2	Santa Cruz	sc-376,861	Mouse	1:500
MRC1	Bioworld	LPO-BS5654	Rabbit	1:1000
Arg1	Santa Cruz	sc-47,715	Mouse	1:500
p-ERK	Santa Cruz	sc-7383	Mouse	1:1000
t-ERK	Santa Cruz	sc-514,302	Mouse	1:1000
p-JNK	Santa Cruz	sc-6254	Mouse	1:1000
t-JNK	Cell Signaling	9252	Rabbit	1:1000
p-p38	Cell Signaling	9211	Rabbit	1:1000
p38	Cell Signaling	9212	Rabbit	1:1000
p-PI3K	Santa Cruz	sc-12,929	Rabbit	1:1000
t-PI3K	Abcam	ab182651	Rabbit	1:1000
p-Akt	Santa Cruz	sc-271,966	Mouse	1:1000
t-Akt	Cell Signaling	9272	Rabbit	1:1000
p-STAT3	Cell Signaling	9131	Rabbit	1:1000
t-STAT3	Cell Signaling	9139	Mouse	1:1000
RARα	Santa Cruz	sc-293,417	Mouse	1:1000
RARβ	Santa Cruz	sc-514,585	Mouse	1:1000
RARγ	Santa Cruz	sc-7387	Mouse	1:1000
p-IκBα	Cell Signaling	9246	Mouse	1:1000
t-IκBα	Cell Signaling	9242	Rabbit	1:1000
p65(C)	Cell Signaling	3033	Rabbit	1:1000
p65(N)	Santa Cruz	sc-7151	Rabbit	1:1000
Histone3	Cell Signaling	9715	Rabbit	1:1000
β-actin	Cell Signaling	4967	Rabbit	1:1000

Table 1. Primary antibodies used in this study.

defined based on isotype-matched control antibodies for each fluorophore. All flow cytometry analyses were performed on singlet-gated populations using identical acquisition settings across samples.

Determination of TNFα, IL-1β, IL-6, PGE2, and NO levels

TNFα, IL-1β, IL-6, and PGE2 levels in the culture media were quantified using enzyme immunoassay (EIA) kits. Briefly, 100 µL of supernatant from treated RAW264.7 cells was added to pre-coated 96-well plates and incubated at room temperature for 2 h. After washing, the plates were incubated with a detection antibody for 2 h. Following additional washes, the conjugate was added and incubated for 30 min, followed by the addition of the substrate solution. The reaction was stopped with 1 N H_2SO_4, and the optical densities were measured at 450 nm using a microplate reader (Perkin Elmer VictorX4, Waltham, MA, USA). Nitrite accumulation in the culture medium, used as a surrogate for NO production, was measured using the Griess reagent. Absorbance was measured at 540 nm using a microplate reader. Fresh culture medium was used as a blank for all experiments.

Subcellular fractionation

A cell fractionation kit was used to extract the cytosolic and nuclear fractions. Briefly, the media from treated cells was aspirated, and the cell pellet was washed with cold 1× PBS and resuspended in 500 µL of ice-cold 1× PBS. A 100 µL aliquot of the cell suspension was set aside in a 1.5 mL tube for the whole cell lysate. The remaining 400 µL was transferred to another 1.5 mL tube and centrifuged at 500 × g for 5 min at 4 ℃. The pellet was resuspended in 500 µL of ice-cold cytoplasm isolation buffer containing 5 µL of protease inhibitor mixture, vortexed for 5 s, and incubated for 5 min at 4 ℃. After centrifugation at 500 × g for 5 min at 4 ℃, the supernatants were saved as the cytosolic fraction. The remaining pellet was resuspended in 500 µL of ice-cold membrane isolation buffer containing 5 µL of protease inhibitor, vortexed for 15 s, and incubated for 5 min at 4 ℃. Following centrifugation at 8,000 × g for 5 min at 4 ℃, the pellet was resuspended in 250 µL of ice-cold nucleus isolation buffer containing 5 µL of protease inhibitor mixture. The resulting supernatants were collected as the nuclear fraction. Successful fractionation was confirmed by the detection of β-actin and histone H3 as cytosolic and nuclear markers, respectively.

p65 immunostaining

The treated cells were fixed in 4% paraformaldehyde (Wako, Cat.163–20145, Japan) for 30 min. After permeabilization with 0.2% TritonX-100 in PBS for 10 min, the cells were incubated with 3% BSA in PBS-T for 1 h to block nonspecific antibody binding. The cells were then incubated with the primary antibody (p65, 1:1000 dilution, Santa Cruz, #sc-7151) in 1% BSA in PBS-T within a humidified chamber overnight at 4℃. After incubation, the cells were washed thrice with PBS for 5 min each. The membranes were then incubated with a secondary antibody (goat anti-rabbit IgG, polyclonal, HRP-conjugated, Enzo, #ADI-SAB-300-J) in 1% BSA for 1 h at room temperature in the dark. After removing the secondary antibody solution, the cells were washed thrice with PBS for 5 min each in the dark. The cells were mounted with a 4',6-diamidino-2-phenylindole (DAPI)-containing mounting medium (VECTASHIELD®) to visualize nuclei. The stained slides were imaged using a Zeiss LSM 700 laser-scanning confocal microscope (Carl Zeiss, Oberkochen, Germany) and analyzed using the ZEN 2010 software (Carl Zeiss). Image quantification was performed using the NIH ImageJ software.

Acute in vivo animal study using LPS-induced septic shock model

C57BL/6J male mice (6 weeks of age, weighing 23.4 ± 0.97 g) were purchased from Orient Bio (Seoul, Korea) and acclimated for 1 week under controlled conditions: temperature, 23 ± 2 ℃; humidity, 40–60%; and a 12-h light/dark cycle. Mice were divided into five groups (n = 6 per group): group 1 mice were treated with vehicle solution (0.5% carboxymethyl cellulose); group 2 mice were intraperitoneally injected with LPS (25 mg/kg) for 6 h; groups 3, 4, and 5 mice were orally administered adapalene (20, 50, and 100 mg/kg, respectively) 1 h before LPS injection for 6 h. After treatment, the mice were anesthetized with isoflurane and subsequently euthanized by cervical dislocation, and the liver tissues were promptly isolated. Some tissues were fixed in 4% paraformaldehyde for staining, whereas others were stored in liquid nitrogen for protein analysis.

To perform immunofluorescence (IF) detection of p-p65 and F4/80, paraffin-embedded liver Sect. (2.5 µm) were deparaffinized and rehydrated. The slides were subjected to the following sequential washes: xylene for 3 min (twice), xylene and 100% ethanol (1:1) for 3 min, 100% ethanol for 3 min (twice), 95% ethanol for 3 min, 70% ethanol for 3 min, and 50% ethanol for 3 min; and finally rinsed with running cold tap water. Rehydrated tissue sections were incubated in Tris-EDTA buffer (10 mM Tris base, 1 mM EDTA, 0.05% Tween 20, pH 9.0) heated to 60℃ for 30 min for antigen retrieval. The sections were blocked with 1% BSA in PBS-T (0.1% TritonX-100 in PBS) for 1 h at room temperature in the dark. Following blocking, sections were incubated overnight at 4 ℃ with primary antibodies: p-p65 (Cell Signaling, #3033) and PE anti-mouse F4/80 (BioLegend, #123110), diluted in blocking buffer. After washing with PBS-T (0.025% TritonX-100 in PBS), the sections were incubated with a secondary antibody (goat anti-rabbit IgG polyclonal antibody; ENZO, #ADI-SAB-300-J) for 1 h at room temperature in the dark. After a final wash with PBS-T, the sections were stained with DAPI and examined using a confocal microscope (LSM-700, Carl Zeiss).

For hematoxylin and eosin (H&E) staining, the rehydrated liver sections were stained with hematoxylin for 3 min, rinsed with tap water, dipped in 95% ethanol, and stained with eosin for 30 s. The sections were washed sequentially with 95% ethanol for 1 min and 100% ethanol for 1 min. They were then incubated in xylene for 1 h and mounted on coverslips and mounting medium. For Picro-Sirius Red staining, rehydrated sections were stained with Picro-Sirius Red solution for 1 h, rinsed with two changes of acetic acid solution and 100% ethanol, and dehydrated twice in 100% ethanol for 1 min. After drying and covering the sections with a mounting medium, images were captured using a light microscope (Axio Imager Z1; Carl Zeiss).

Chronic in vivo animal study using HFD-induced obese mice

To further investigate the anti-inflammatory and beneficial effects of adapalene, C57BL/6J male mice (6 weeks of age) were fed an HFD (60% fat) for 4 weeks, after their body weight increased to 31.9 ± 1.62 g. Adapalene (10 or 50 mg/kg) was orally administered once daily for 3 weeks. The subsequent procedures were performed as described above, except that euthanasia was performed under deep isoflurane anesthesia. Oil Red O staining of the liver tissues was performed as previously described[24] . All animal procedures adhered to the Guide for the Care and Use of Laboratory Animals published by the U.S. National Institutes of Health (NIH Publication No. 85 – 23, revised in 2011). This study was approved by the Animal Care and Use Committee of the Gachon University, Seongnam, Korea (Approval Numbers: LCDI-2020-0028, LCDI-2020-0120), and is reported in accordance with ARRIVE guidelines.

Statistical analysis

The statistical significance of differences versus respective controls was established using one-way analysis of variance (ANOVA) followed by Tukey's post-hoc test. Results are expressed as the means ± SDs of three separate experiments, and statistical significance was set at $p < 0.05$.

Results

Inhibition of LPS-induced inflammation by adapalene in murine macrophages

To investigate the anti-inflammatory effects of adapalene in murine macrophages, RAW264.7 cells were treated with LPS (100 ng/mL) in the presence or absence of adapalene. Based on a combination of preliminary concentration–response experiments and previously published studies[22], we selected adapalene concentrations ranging from 10 to 1000 nM. Adapalene inhibited the mRNA expression of pro-inflammatory markers, including TNFα, IL-6, IL-1β, iNOS and COX-2 in a concentration-dependent manner (Fig. 1A). Similarly, LPS significantly

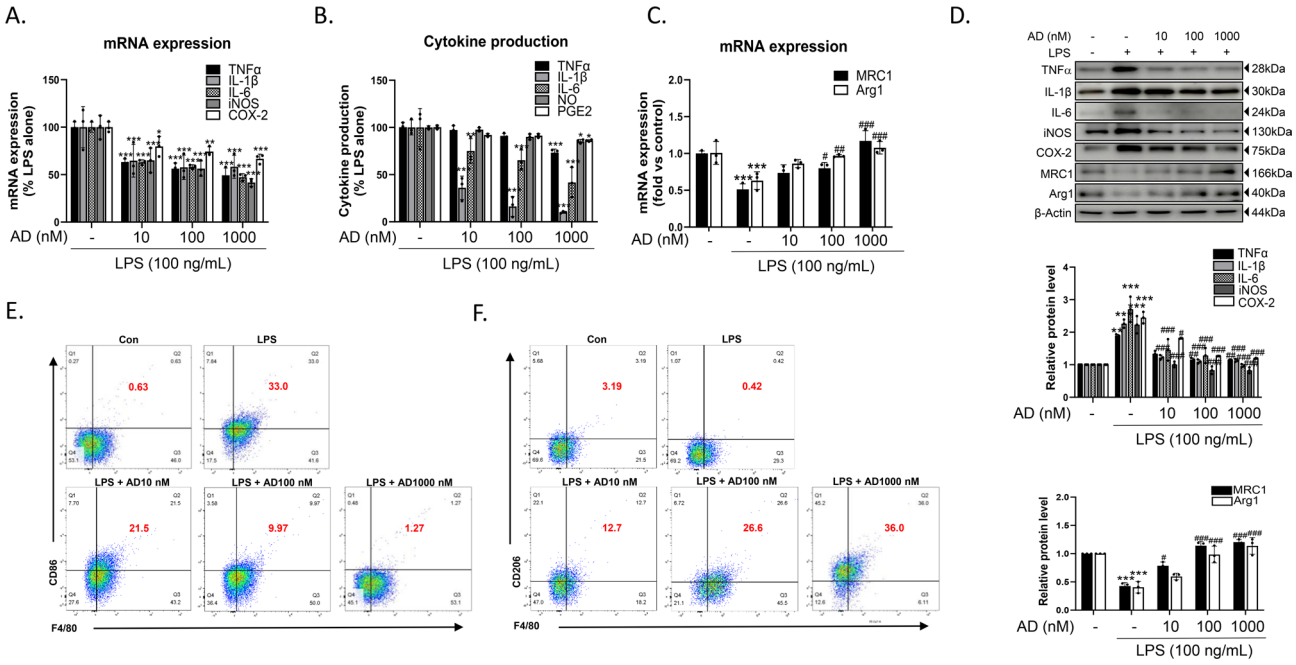

Fig. 1. Adapalene reduces LPS-stimulated pro-inflammatory cytokine production in murine macrophages. (A) RAW264.7 cells were treated with adapalene (10, 100, or 1000 nM) for 1 h, followed by LPS (100 ng/mL) for 24 h. Total RNA was prepared for qRT-PCR analysis of TNFα, IL-1β, IL-6, iNOS, and COX-2, and mRNA levels were determined using gene-specific primers. (B) Following pretreatment with or without adapalene, TNFα, IL-6, and IL-1β levels in culture media were quantified using ELISA. NO and PGE2 levels in culture media were quantified using a Griess reaction assay and EIAs, respectively. $^{*}P < 0.05$, $^{**}P < 0.01$, and $^{***}P < 0.001$ vs. LPS alone. (C) mRNA expression of M2 markers MRC1 and Arg1 was determined using RT-qPCR. (D) Protein levels of pro-inflammatory cytokines and M2 markers were determined using western blot analysis. Band densities were analyzed using ImageJ software, normalized to β-actin, and the results are shown in lower panel. Membranes were cut prior to antibody incubation; all available uncropped images are provided in the Supplementary Information. Original full-length images for certain replicates are unavailable due to loss of original acquisition files. $^{*}P < 0.05$, $^{**}P < 0.01$, and $^{***}P < 0.001$ vs. control; $^{\#}P < 0.05$ and $^{\#\#}P < 0.01$ vs. LPS alone. (E, F) After treatment of RAW264.7 cells with LPS and adapalene, immunofluorescence analysis of F4/80 positive remove ($^{+}$)macrophages was carried out. Flow cytometry data were analyzed using FlowJo Software v11.0 (Ashland, OR, USA). The experiment was performed three times in triplicate and results are presented as the mean ± S.D. of three independent experiments. A complete flow cytometry gating strategy and isotype control data are shown in Supplementary Fig. 1E. AD; adapalene.

increased the production of pro-inflammatory cytokines such as TNFα, IL-6, and IL-1β, whereas adapalene effectively suppressed these LPS-induced effects (Fig. 1B). LPS-induced NO and PGE2 production was also reduced by adapalene, albeit to a lesser extent; however, the effects remained statistically significant. Conversely, adapalene restored the LPS-suppressed mRNA expression of anti-inflammatory markers such as MRC1 and Arg1 in a concentration-dependent manner (Fig. 1C). A similar trend was observed at the protein level, where adapalene reduced the pro-inflammatory cytokine levels and enhanced the anti-inflammatory marker levels (Fig. 1D). Consistent with these findings, FACS analysis revealed that adapalene significantly reduced the expression of the M1- associated marker CD86, while increasing the expression of the M2-associated marker CD206 in LPS-stimulated RAW264.7 macrophages (Figs. 1E and F). These findings suggested that adapalene exerts dual anti-inflammatory effects in murine macrophages by inhibiting LPS-induced pro-inflammatory responses and restoring LPS-suppressed anti-inflammatory responses. Adapalene alone had little effect on the expression of pro-inflammatory and M2 markers (results not shown).

Signaling pathways involved in adapalene-mediated anti-inflammatory actions

Several signaling pathways, including the MAPK and PI3K/Akt pathways, have been implicated in LPS-induced macrophage inflammation and overlap with retinoid signaling[25]. To investigate the signaling pathways involved in adapalene action, we first examined its effects on the MAPK pathway using western blot analysis. As expected, LPS stimulated the phosphorylation of ERK, JNK, and p38 MAPK, whereas adapalene reduced their phosphorylation in a concentration-dependent manner (Fig. 2A). Adapalene alone did not affect the phosphorylation status of these signaling mediators (data not shown).

Next, we evaluated the effects of adapalene on the PI3K/Akt signaling pathway. The results showed that adapalene attenuated the phosphorylation of both PI3K and Akt (Fig. 2B), indicating that the anti-inflammatory effects of adapalene may arise from its ability to interfere with multiple LPS-activated signaling pathways, specifically MAPK and PI3K/Akt pathways. Interestingly, STAT3 phosphorylation has been identified as a key mediator of M2 macrophage polarization, promoting the transcription of MRC1 and Arg1, which are

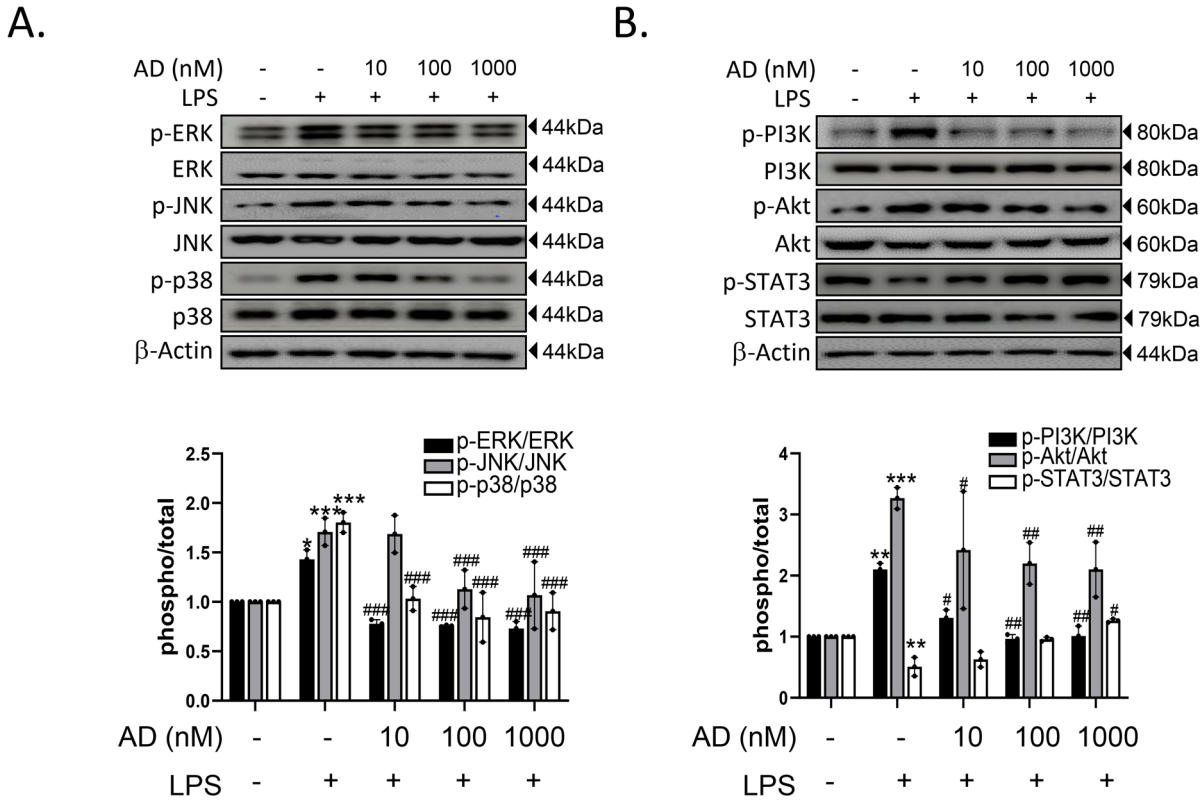

Fig. 2. Adapalene reduces LPS-stimulated MAPK and PI3K/Akt signaling in murine macrophages. RAW264.7 cells were pretreated with or without adapalene (10, 100, or 1000 nM) for 1 h and then stimulated with LPS (100 ng/mL) for 30 min. Total cellular proteins were resolved using SDS-PAGE and detected using specific antibodies against p-p38, p38, p-JNK, JNK, p-ERK, ERK (A), p-Akt, Akt, p-PI3K, PI3K, p-STAT3, and STAT3 (B). β-actin was used as an internal control. Membranes were cut prior to antibody incubation; all available uncropped images are provided in the Supplementary Information. Original full-length images for certain replicates are unavailable due to loss of original acquisition files. Representative results are shown and density analysis is presented as the mean ± S.D. of three independent experiments in lower panel. AD; adapalene, $^{*}P<0.05$, $^{**}P<0.01$, and $^{***}P<0.001$ vs. control; $^{\#}P<0.05$ and $^{\#\#}P<0.01$ vs. LPS alone.

two well-established M2 markers. Consistent with this finding, we confirmed that adapalene induced STAT3 phosphorylation, which was accompanied by an increase in the M2 macrophage population (Fig. 2B).

Elucidation of RAR subtypes involved in the mechanism of action of adapalene

To determine whether RAR is implicated in the anti-inflammatory effects of adapalene and, if so, which RAR subtype is involved, the expression of RAR subtypes in RAW264.7 cells was analyzed using western blotting and RT-qPCR. As shown in Fig. 3A, RARα was the predominant subtype, followed by RARβ, whereas RARγ expression was barely detectable. Since adapalene exhibits a high affinity for RARβ and RARγ, but not RARα[21,22], we focused on the role of RARβ in mediating the effects of adapalene by performing RARβ knockdown experiments.

Transfection with RARβ-specific siRNA (100 nM) reduced RARβ mRNA and protein levels by 62–65% compared to control siRNA (Fig. 3B). The suppressive effects of adapalene on LPS-stimulated mRNA expression of pro-inflammatory mediators were significantly diminished by RARβ knockdown (Fig. 3C). Consistent with this, the reduction in protein levels of pro-inflammatory mediators in the presence of adapalene was reversed almost to the levels observed with LPS alone upon RARβ knockdown (Fig. 3D). These findings indicate that the anti-inflammatory effects of adapalene are primarily mediated by RARβ. Moreover, adapalene restored the suppressed mRNA and protein levels of M2 markers induced by LPS, and these effects were abolished by RARβ siRNA transfection (Figs. 3C and D).

To further validate the role of RARβ in the mechanism of action of adapalene, we used the RARβ-selective antagonist LE135. Consistent with the RARβ knockdown results, LE135 markedly reversed the anti-inflammatory effects of adapalene in a concentration-dependent manner. LE135 counteracted the adapalene-induced reduction in the mRNA and protein levels of pro-inflammatory markers and reversed the increase in the mRNA and protein levels of anti-inflammatory markers (Figs. 4A and B). These results confirm that RARβ-mediated macrophage polarization toward the M2 phenotype is crucial for the anti-inflammatory effects induced by adapalene.

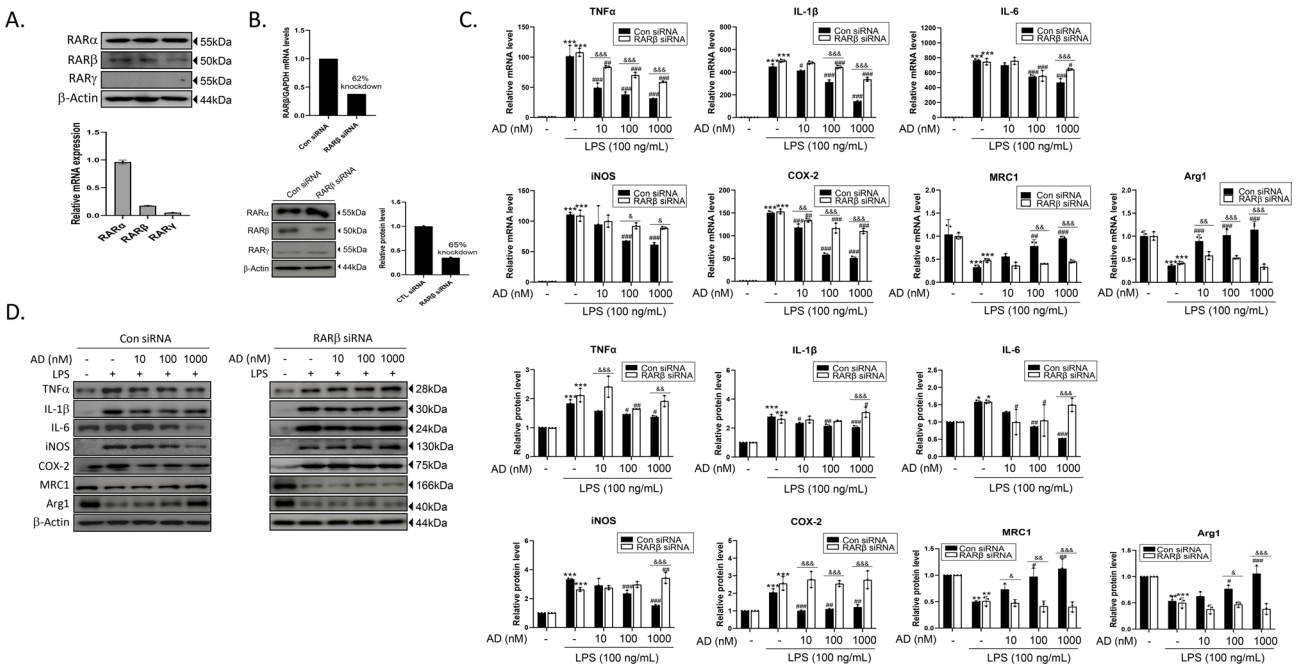

Fig. 3. RARβ knockdown reverses protective effects of adapalene against LPS-stimulated pro-inflammatory cytokine production. (A) The protein (upper) and mRNA (lower) levels of RAR subtypes in RAW264.7 cells were determined using western blot analysis and RT-qPCR, respectively. (B) RAW264.7 cells were transfected with either control siRNA or RARβ siRNA (100 nM), and the extent of RARβ knockdown was determined using RT-qPCR and western blot analysis. (C, D) After gene silencing using RARβ siRNA, RAW264.7 cells were treated with adapalene (10, 100, or 1000 nM) for 24 h, and the levels of pro-inflammatory markers were determined using RT-qPCR (C) and by western blot analysis (D). Membranes were cut prior to antibody incubation; all available uncropped images are provided in the Supplementary Information. Original full-length images for certain replicates are unavailable due to loss of original acquisition files. Density analyses are shown in the right panel. The experiment was performed three times in triplicate and results are presented as the mean ± S.D. of three independent experiments. AD; adapalene, $^{*}P<0.05$, $^{**}P<0.01$, and $^{***}P<0.001$ vs. control; $^{\#}P<0.05$, $^{\#\#}P<0.01$, and $^{\#\#\#}P<0.001$ vs. LPS alone; $^{\&}P<0.05$, $^{\&\&}P<0.01$, and $^{\&\&\&}P<0.001$ vs. control siRNA.

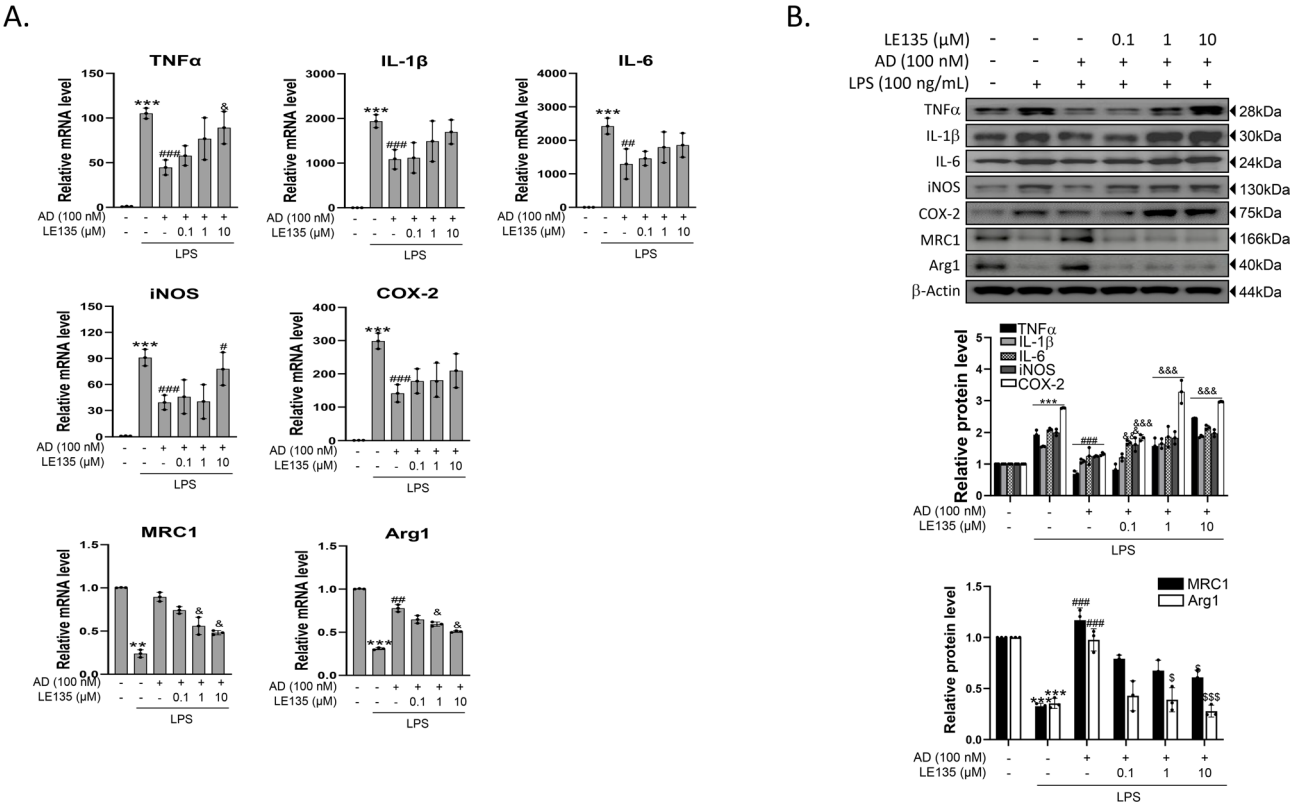

Fig. 4. RARβ antagonist reverses protective effects of adapalene against LPS-stimulated pro-inflammatory cytokine production. RAW264.7 cells were co-treated with LE135 (0.1, 1, or 10 μM) and adapalene (100 nM), and then exposed to LPS (100 ng/mL) for 24 h. The levels of pro-inflammatory markers were determined using RT-qPCR (A) and western blot analysis (B). Membranes were cut prior to antibody incubation; all available uncropped images are provided in the Supplementary Information. Original full-length images for certain replicates are unavailable due to loss of original acquisition files. Density analysis is shown in the lower panel. The experiment was performed three times in triplicate and results are presented as the mean ± S.D. of three independent experiments. AD, adapalene; ns, not significant. $^{**}P<0.01$ and $^{***}P<0.001$ vs. control; $^{\#}P<0.05$, $^{\#\#}P<0.01$, and $^{\#\#\#}P<0.001$ vs. LPS alone; $^{\&}P<0.05$, $^{\&\&}P<0.01$, and $^{\&\&\&}P<0.001$ vs. AD plus LPS.

RARβ downstream signaling in adapalene actions

The effects of RARβ siRNA or the RARβ antagonist LE135 on adapalene-induced suppression of the MAPK and PI3K/Akt pathways were evaluated. RARβ siRNA attenuated the adapalene-mediated inactivation of MAPK in response to LPS stimulation (Fig. 5A). Similarly, LE135 treatment reversed the inhibitory effects of adapalene on MAPK inactivation (Fig. 5C). Likewise, the inhibitory effects of adapalene on LPS-induced phosphorylation of PI3K/Akt, as well as the restoration of STAT3 phosphorylation suppressed by LPS, were abolished by either RARβ siRNA or LE135 treatment (Figs. 5B and D).

As NF-κB activation is a key regulator of inflammatory responses, the effects of adapalene on LPS-induced NF-κB activation were also examined. Adapalene reduced LPS-induced IκBα phosphorylation (Figs. 6A and C), accompanied by a decrease in p65 nuclear translocation (Figs. 6B and D). Both effects were reversed by RARβ siRNA (Fig. 6A and B) or LE135 (Figs. 6C and D). Furthermore, NF-κB immunostaining with an anti-p65 antibody revealed that LPS-induced nuclear translocation of p65 was significantly blocked by adapalene (Fig. 6E). However, these effects were completely abolished by treatment with either RARβ siRNA or LE135 (Figs. 6F and G). Collectively, these results demonstrate that adapalene exerts potent anti-inflammatory effects in macrophages primarily through RARβ activation. This activation leads to the suppression of multiple parallel signaling pathways, including MAPK, PI3K/Akt, and NF-κB inactivation.

In vivo anti-inflammatory effects of adapalene in LPS-induced sepsis model and HFD-induced obesity model

Two complementary in vivo models were employed to assess the generalizability of adapalene's immunomodulatory effects across distinct inflammatory settings: an LPS-induced sepsis model representing acute systemic inflammation and an HFD-induced obesity model reflecting chronic metabolic inflammation, both of which are critically driven by macrophage polarization imbalance.

Intraperitoneal injection of LPS (25 mg/kg) into C57BL/6J mice elevated serum IL-1β, IL-6, and TNFα levels, along with increased mRNA expression of these cytokines in the liver. Consistent with the in vitro findings, oral administration of adapalene (1 h before induction) dose-dependently reduced LPS-induced production of

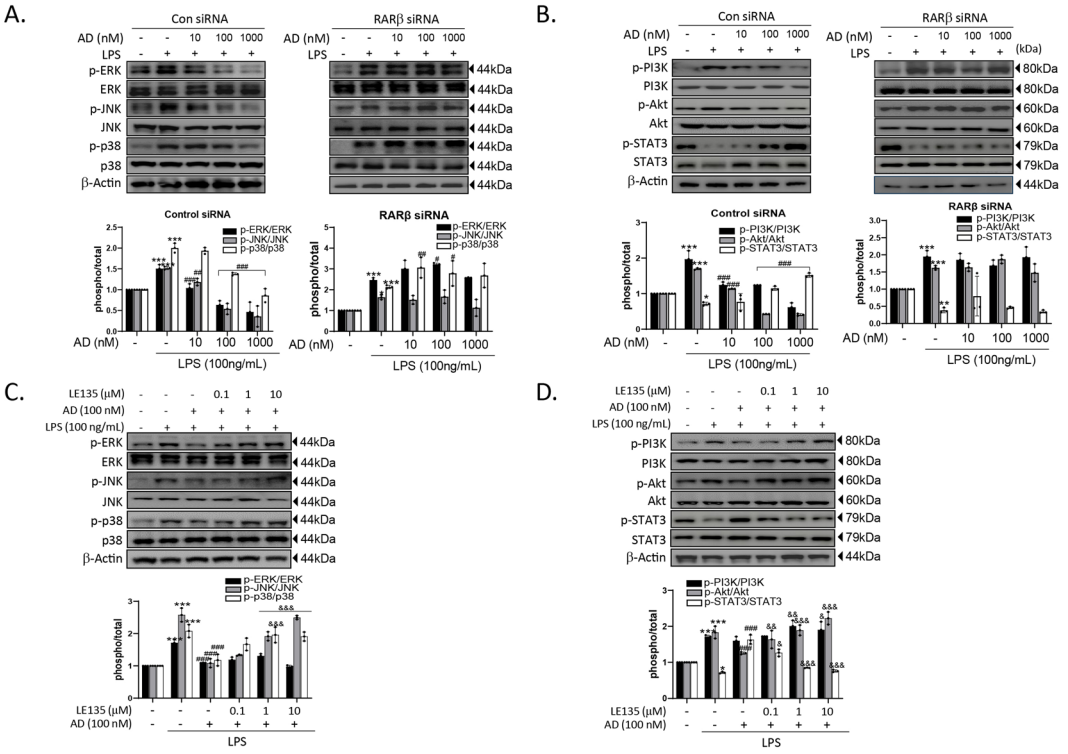

Fig. 5. RARβ mediates adapalene-induced anti-inflammatory signaling. (A, B) RAW264.7 cells were transfected with control siRNA or RARβ siRNA (100 nM), and then treated with LPS in the presence or absence of adapalene for 24 h. Total cellular proteins were resolved using SDS-PAGE and detected using the specific antibodies p-p38, p38, p-JNK, JNK, p-ERK, and ERK (A) and specific antibodies p-Akt, Akt, p-PI3K, PI3K, p-STAT3, and STAT3 (B). (C, D) RAW264.7 cells were treated in the presence or absence of LE135 (0.1–10 μM) with or without adapalene and LPS for 24 h. Total cellular proteins were resolved using SDS-PAGE and detected using specific antibodies p-p38, p38, p-JNK, JNK, p-ERK, and ERK (C) and specific antibodies p-Akt, Akt, p-PI3K, PI3K, p-STAT3, and STAT3 (D). Membranes were cut prior to antibody incubation; all available uncropped images are provided in the Supplementary Information. Original full-length images for certain replicates are unavailable due to loss of original acquisition files. Density analyses are shown in lower panel. The experiment was performed three times in triplicate and results are presented as the mean ± S.D. of three independent experiments. AD; adapalene, $^{*}P<0.05$, $^{**}P<0.01$, and $^{***}P<0.001$ vs. control; $^{\#}P<0.05$, $^{\#\#}P<0.01$, and $^{\#\#\#}P<0.001$ vs. LPS alone; $^{\&}P<0.05$, $^{\&\&}P<0.01$, and $^{\&\&\&}P<0.001$ vs. AD plus LPS.

pro-inflammatory cytokines in both the serum and liver (Figs. 7A–C). Notably, adapalene dose-dependently increased RARβ levels, with minimal effects on RARα and RARγ (Fig. 7C). Additionally, adapalene attenuated LPS-induced activation of the MAPK and PI3K/Akt pathways and restored STAT3 activity in the liver (Fig. 7D). This was accompanied by a reduction in phosphorylated NF-κB levels and a decrease in F4/80-positive macrophages (Figs. 7E–G).

Histological analysis using H&E staining revealed that the distorted hepatic structure observed in LPS-treated mice was ameliorated in the adapalene-treated group (Fig. 7H), along with reduced serum ALT and AST levels (Fig. 7A). While LPS injection alone resulted in 100% mortality within 48 h, pre-treatment with adapalene dose-dependently increased the survival rates, achieving up to 80% survival against LPS-induced septic shock (Fig. 7I). Interestingly, adapalene reduced LPS-induced mRNA and protein levels of the fibrosis markers Col1a1 and αSMA (Fig. 7J), indicating an anti-fibrotic effect. In addition, the increased collagen deposition caused by LPS was also decreased by adapalene as indicated by the Picro-Sirius red staining (Fig. 7K). These findings demonstrated that adapalene effectively suppressed LPS-induced inflammatory and fibrotic responses in vivo.

Given that adipose tissue inflammation is a critical contributor to insulin resistance and metabolic disorders[25,26], we further investigated the anti-inflammatory effects of adapalene following chronic administration in HFD-induced obesity mouse model. Adapalene was orally administered once daily for 3 weeks. As shown in Figs. 8A and C, adapalene reduced the mRNA and protein levels of pro-inflammatory markers, while increasing the levels of anti-inflammatory markers. Furthermore, the enhanced phosphorylation of MAPK and PI3K/Akt observed in HFD-fed mice was significantly diminished in the adapalene-treated group, with increased STAT3 phosphorylation (Figs. 8A and B). In addition, hepatic triglyceride accumulation induced by HFD was markedly reduced in adapalene-treated mice, as confirmed by Oil Red O staining (Fig. 8D). These results suggest that adapalene suppresses the pro-inflammatory responses associated with HFD-induced obesity, accompanied by M2 macrophage polarization. This anti-inflammatory action may ameliorate pathological conditions related to inflammation and metabolic disorders. Additionally, in the adapalene-treated groups, the mRNA and protein

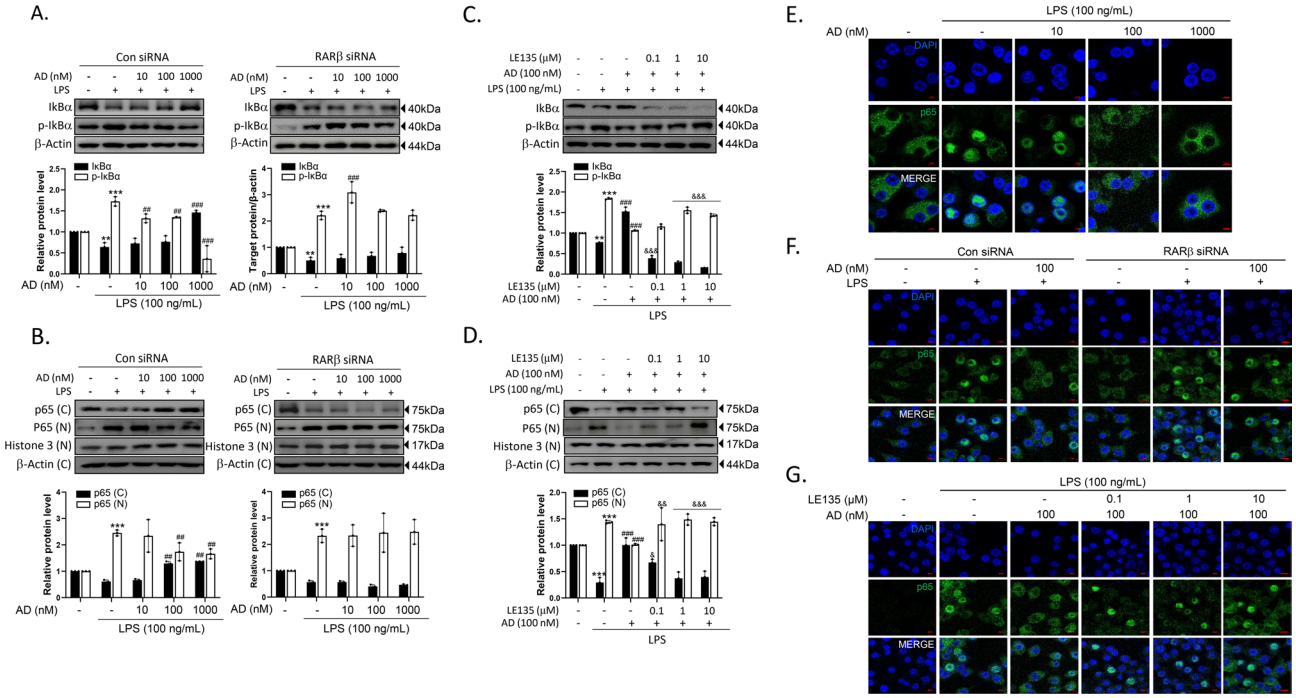

Fig. 6. RARβ mediates adapalene-induced NF-κB suppression after LPS stimulation in RAW264.7 cells. (A, B) RAW264.7 cells were transfected with control siRNA or RARβ siRNA (100 nM), and then treated with LPS in the presence or absence of adapalene for 24 h. Total cellular proteins were resolved using SDS-PAGE and detected using specific antibodies p-IκBα and IκBα (A) and subcellular fractionated nuclear and cytosol detection using p65 specific antibodies (B). (C, D) RAW264.7 cells were treated in the presence or absence of LE135 (0.1–10 μM) with or without adapalene and LPS for 24 h. Total cellular proteins were resolved using SDS-PAGE and detected using specific antibodies p-IκBα and IκBα (C) and subcellular fractionated nuclear and cytosol detection using p65 specific antibodies (D). Membranes were cut prior to antibody incubation; all available uncropped images are provided in the Supplementary Information. Original full-length images for certain replicates are unavailable due to loss of original acquisition files. Density analyses are shown in lower panel. (E) IF staining for p65 was performed after RAW264.7 cells were treated with different concentrations of adapalene. (F, G) IF staining for p65 was carried out after RAW264.7 cells were treated with different concentrations of adapalene in the presence of either RARβ siRNA (F) or LE135 (G). The experiment was performed three times in triplicate and results are presented as the mean ± S.D. of three independent experiments. AD; adapalene, $^{*}P<0.05$, $^{**}P<0.01$, and $^{***}P<0.001$ vs. control; $^{\#}P<0.05$, $^{\#\#}P<0.01$, and $^{\#\#\#}P<0.001$ vs. LPS alone; $^{\&}P<0.05$ and $^{\&\&}P<0.01$ vs. AD plus LPS.

levels of fibrosis markers were reduced (Fig. 8E and F), which was consistent with the findings in the LPS-induced sepsis model. These effects further highlighted the protective role of adapalene against HFD-induced hepatic damage.

Discussion

Retinoids, a group of compounds with biological activities similar to those of Vitamin A, play a pivotal role in numerous essential biological processes, including innate immunity, primarily through RAR binding. However, their effect on the inflammatory response of macrophages remains unclear. In this study, we examined the effects of adapalene, a third-generation retinoid, on LPS-induced inflammatory responses in murine macrophages and explored the underlying mechanisms of its action. Our findings can be summarized as follows: (1) Adapalene suppressed the LPS-induced pro-inflammatory effects in murine macrophages. (2) These effects were mediated predominantly through RARβ activation, which led to the inactivation of the MAPK and PI3K/Akt pathways, as well as NF-κB inactivation. (3) Adapalene promoted M2 polarization in murine macrophages through RARβ-mediated STAT3 phosphorylation. (4) The anti-inflammatory actions of adapalene were confirmed in vivo using both LPS-induced sepsis and HFD-induced obesity mouse models. The proposed working model for the mechanism of action of adapalene is presented in Fig. 9.

Appropriate macrophage function is critical for effective immune and inflammatory responses. Moreover, obesity-induced low-grade inflammation in adipose tissue macrophages contributes to insulin resistance, which is a hallmark of metabolic diseases, highlighting the potential of modulating macrophage activity as an effective therapeutic strategy. Among the various approaches used to achieve anti-inflammatory effects, retinoids have demonstrated significant potential, although the precise mechanisms of their actions remain poorly understood. Several examples of retinoid-induced anti-inflammatory mechanisms have been reported. Fawzy et al[27] demonstrated that retinoids, such as retinal, retinol, retinoic acid, and retinol acetate, inhibit phospholipase

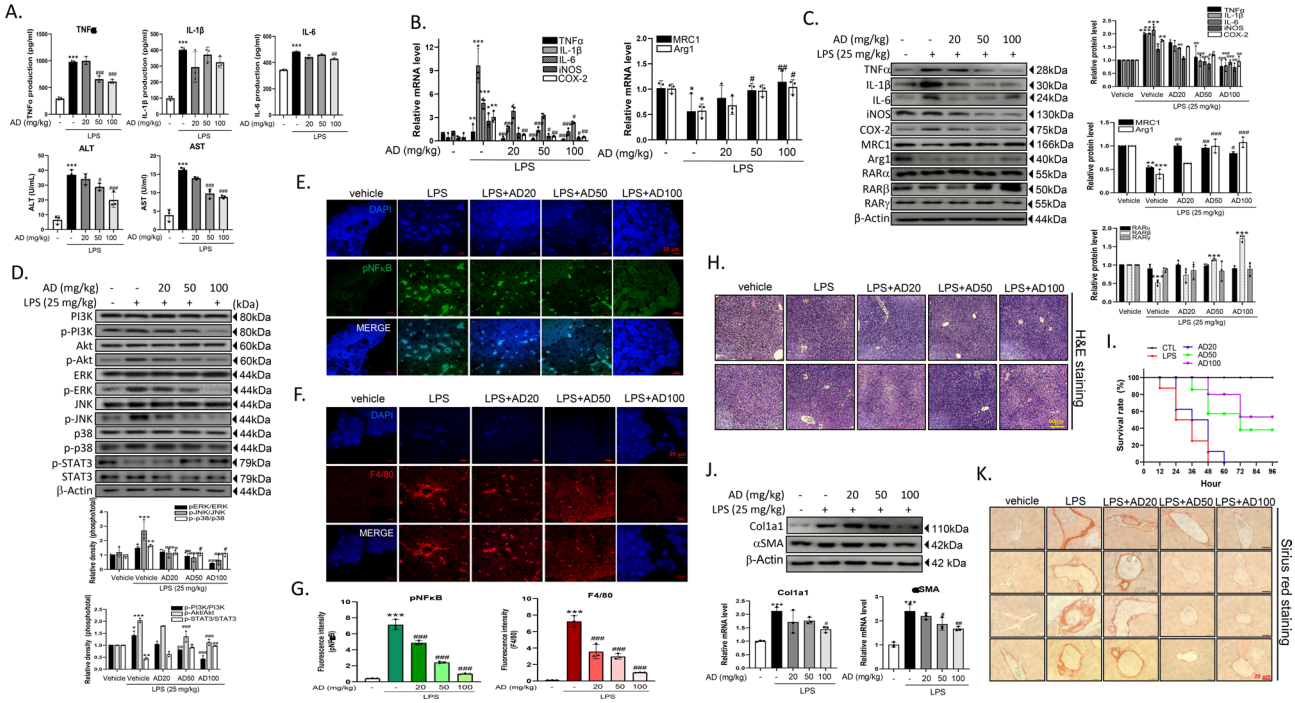

Fig. 7. In vivo anti-inflammatory effects of adapalene in LPS-induced septic shock model. Six mice per group were treated with vehicle only or adapalene (20, 50, or 100 mg/kg, *p.o.*) for 1 h and then injected with LPS (25 mg/kg, *i.p.*). Serum and liver samples were collected from each mouse after 6 h. (A, B) TNFα, IL-6, and IL-1β protein in serum (A) and mRNA levels of TNFα, IL-1β, IL-6, iNOS, and COX-2 in liver (B) were determined using EIA and qRT-PCR, respectively. (C) TNFα, IL-1β, IL-6, iNOS, COX-2, MRC1, Arg1, RARα, RARβ, and RARγ protein levels in liver were determined using western blot. Membranes were cut prior to antibody incubation; all available uncropped images are provided in the Supplementary Information. Original full-length images for certain replicates are unavailable due to loss of original acquisition files. Density analysis is shown in the right panel. (D) Protein levels of p38, p-p38 MAPK, ERK, p-ERK, JNK, p-JNK, PI3K, p-PI3K, Akt, p-Akt, STAT3, and p-STAT3 in the liver were determined using western blotting. Density analysis is shown in the lower panel. Results are presented as the means ± S.D. of six mice. Representative images of p-NF-κB staining (E), F4/80 staining (F), H&E staining (H), and Picro-Sirius Red staining (K) of liver tissues were shown. Quantitative analysis of p-NF-κB and F4/80 staining was performed using ImageJ software (G). The survival rate after adapalene administration in LPS-induced sepsis is shown (I). Hepatic mRNA and protein levels of fibrosis markers were determined (J). AD; adapalene, $^{*}P<0.05$, $^{**}P<0.01$, and $^{***}P<0.001$ vs. control; $^{\#}P<0.05$, $^{\#\#}P<0.01$, and $^{\#\#\#}P<0.001$ vs. LPS alone.

A2 in the human synovial fluid, reducing arachidonic acid, a precursor of inflammatory metabolites. Similarly, retinoids inhibit COX-2 activity in mouse peritoneal macrophages[28]. ATRA, an endogenous RAR ligand, suppresses LPS-induced NF-κB activation[29], whereas Vitamin A deficiency is associated with increased inflammatory responses through heightened NF-κB signaling, suggesting a critical interaction between RAR and NF-κB signaling[30–32]. Additionally, ATRA has been shown to directly inhibits pro-inflammatory cytokine production in activated monocytes and macrophages[18,19,33]. However, the specific effects of ATRA on macrophage-mediated inflammation, particularly in relation to RAR-mediated signaling pathways, remain unclear. Previous studies have indicated that different RAR subtypes play context-dependent roles in the anti-inflammatory effects observed in macrophages and immune cells[18,34,35]. In this study, we selected adapalene as an RAR ligand due to its established clinical use and demonstrated that RARβ plays a critical role in the anti-inflammatory effects observed in activated RAW264.7 cells.

Although adapalene is known to exhibit relatively high affinity for RARγ, the contribution of this receptor to the observed anti-inflammatory effects appears limited in our experimental system. In RAW264.7 macrophages, RARγ expression was barely detectable compared with RARα and RARβ, consistent with previous reports demonstrating cell type-specific and context-dependent expression patterns of RAR isoforms in immune cells[14,34,36]. This low expression profile guided our mechanistic focus toward RARβ as the predominant mediator of adapalene's actions in macrophages. Nevertheless, RARγ has been implicated in immune regulation in other cellular contexts, particularly in epithelial and stromal cells, where it plays important roles in retinoid signaling and inflammatory modulation. Therefore, it remains possible that RARγ-dependent effects of adapalene may emerge in macrophage subsets, differentiation states, or tissue microenvironments characterized by higher RARγ expression. Future studies employing genetic or isoform-specific approaches will be required to clarify the potential contribution of RARγ to retinoid-mediated immune regulation.

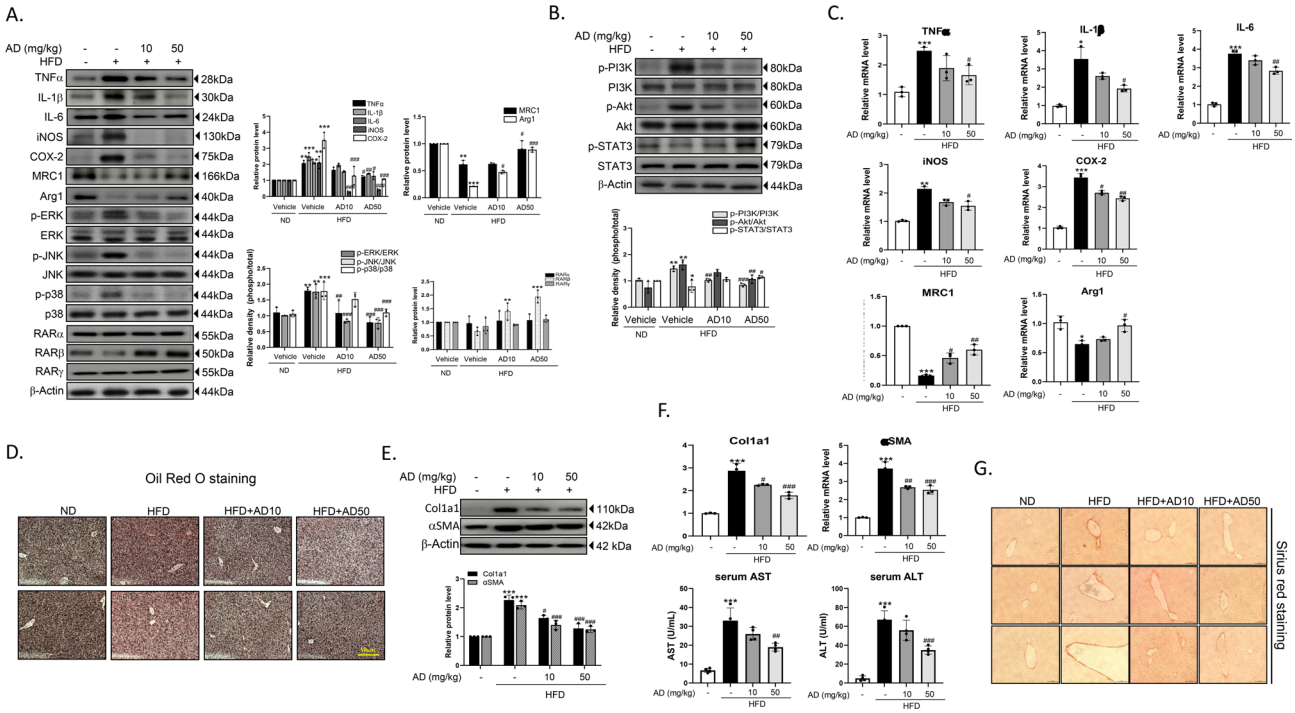

Fig. 8. In vivo anti-inflammatory effects of adapalene in HFD-induced obesity model. Adapalene (10 or 50 mg/kg) was orally administered once daily to HFD-induced obese mice ($n = 10$ per group) for 3 weeks. On the last day of administration, serum and liver samples were collected from each mouse. (A) TNFα, IL-1β, IL-6, iNOS, COX-2, MRC1, Arg1, p38, p-p38 MAPK, ERK, p-ERK, JNK, p-JNK, RARα, RARβ, and RARγ protein levels in the liver were determined using western blotting. Density analysis is shown in the right panel. (B) PI3K, p-PI3K, Akt, p-Akt, STAT3, and p-STAT3 protein levels in the liver were determined using western blotting. Membranes were cut prior to antibody incubation; all available uncropped images are provided in the Supplementary Information. Original full-length images for certain replicates are unavailable due to loss of original acquisition files. Density analysis is shown in the lower panel. (C) TNFα, IL-6, IL-1β, COX-2, iNOS, MRC1, and Arg1 mRNA levels in the liver were determined using qRT-PCR. (D) Representative images of Oil Red O staining and Picro-Sirius Red staining (G) of liver tissues are shown. Results are presented as the means ± S.D. of eight mice. (E, F) Hepatic protein levels (E), mRNA levels of fibrosis markers (F) and serum ALT and AST levels (F) were determined. AD; adapalene, $^{*}P < 0.05$, $^{**}P < 0.01$, and $^{***}P < 0.001$ vs. control; $^{\#}P < 0.05$, $^{\#\#}P < 0.01$, and $^{\#\#\#}P < 0.001$ vs. LPS alone.

Retinoic acids regulate gene transcription by directly binding to RAR in the nucleus, and subsequently interacting with the RARE promoter sequences of target genes through the formation of heterodimers with RXR or PPAR. Interestingly, the activation of protein kinases, such as PKA, PKC, and MAPK, is also implicated in retinoid-mediated transcriptional regulation[25]. In the present study, adapalene reduced LPS-stimulated phosphorylation of MAPK and PI3K in an RARβ-dependent manner. Similarly, it has been shown that ATRA-induced changes in MAPK phosphorylation are mediated through RARβ[37]. Based on our findings, the anti-inflammatory effects of adapalene are at least partly mediated through RARβ-mediated non-genomic pathways.

LPS, a primary component of endotoxins in gram-negative bacterial cell walls, also functions as an endogenous stimulator of inflammation[38]. It is well-established that NF-κB and AP-1 are pivotal transcription factors involved in LPS-stimulated inflammatory responses in macrophages[39,40]. In this study, adapalene attenuated LPS-induced phosphorylation of IκBα, thereby suppressing NF-κB activation, an effect that was reversed by RARβ blockade. These results support the hypothesis that adapalene interferes with LPS-induced inflammatory signaling in murine macrophages through RARβ activation, leading to the inactivation of MAPK, PI3K/Akt, and NF-κB pathways.

Given the critical role of macrophages in the regulation of immune responses and metabolism, imbalanced macrophage polarization can contribute to the development of metabolic and inflammatory disorders. A key therapeutic implication of the present study is the dual regulatory effect of adapalene on macrophage polarization. Adapalene not only suppresses pro-inflammatory M1 macrophage activation but also actively promotes anti-inflammatory M2 polarization, highlighting its capacity to coordinately modulate macrophage plasticity. This balanced regulation is increasingly recognized as essential for the effective resolution of inflammation and restoration of metabolic homeostasis, rather than simple inhibition of inflammatory signaling alone[41,42]. By simultaneously attenuating inflammatory responses and enhancing reparative macrophage programs through RARβ-dependent mechanisms, adapalene represents a promising strategy for targeting macrophage-driven inflammatory and metabolic diseases.

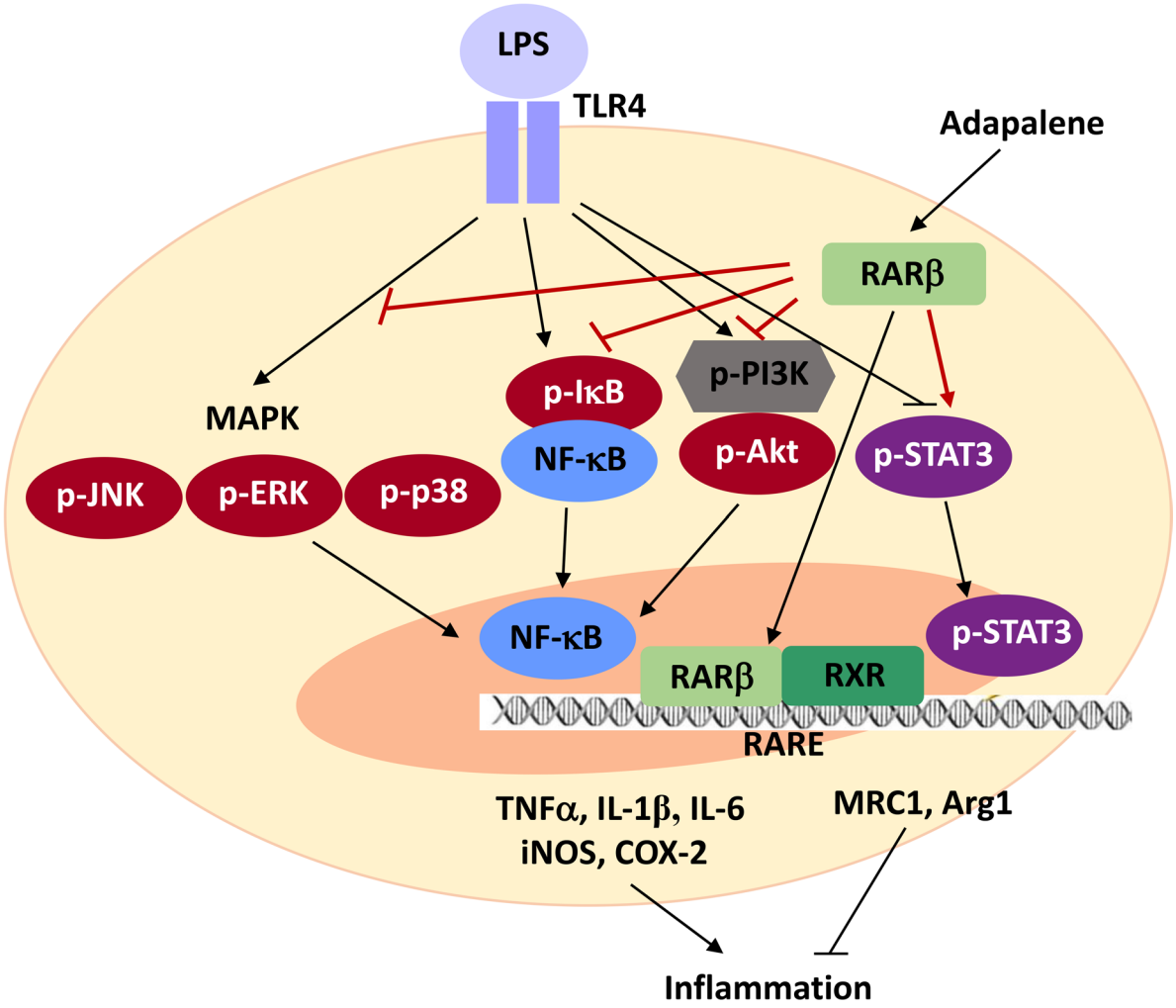

Fig. 9. Proposed working model of the mechanism of action of adapalene. Adapalene produces anti-inflammatory effects through dual mechanisms involving the suppression of the M1-mediated inflammatory response and induction of the M2-mediated anti-inflammatory response. Both actions are mediated through RARβ activation, followed by MAPK and PI3K/Akt inactivation, and NF-κB inactivation (M1 response) as well as by STAT3 phosphorylation (M2 response).

Sepsis, a life-threatening condition characterized by dysregulated immune responses to severe infections, is a clear example of this strategy. Inhibition of M1 macrophages has been shown to rescue from tissue damage and mortality by inflammatory factors production[43] Simultaneously, promoting M2 polarization can reduce the levels of inflammatory mediators and improve survival rates[44,45]. Recent studies have demonstrated that ATRA exerts anti-inflammatory effects by modulation M1-to- M2 polarization[15–17]. Interestingly, fenretinide, a synthetic retinoid, exhibits anti-inflammatory effects through PPARγ-mediated regulation of macrophage polarization[46].

The activation of various signaling pathways, including the PI3K/Akt, JAK/STAT6, STAT3, and TGF1/SMAD-dependent pathways, is known to drive M2 polarization. In the present study, adapalene improved survival outcomes in sepsis models, reduced pro-inflammatory cytokine levels, and decreased liver damage, highlighting its protective effects against acute liver failure. The protective effects of adapalene in LPS-induced septic shock were attributed to its dual modulation of macrophage polarization, simultaneously inhibiting M1 macrophages and inducing M2 macrophages, resulting in enhanced survival and reduced inflammatory damage.

Chronic obesity often leads to ectopic fat accumulation, which causes systemic insulin resistance[47]. In particular, hepatic lipid accumulation is associated with severe conditions such as non-alcoholic fatty liver disease, fibrosis, and cirrhosis. Consequently, anti-inflammatory agents are widely recognized as potential therapeutics for slowing the progression of metabolic diseases. In this study, we demonstrated that oral administration of adapalene (10 and 50 mg/kg) for 3 weeks ameliorated HFD-induced inflammatory responses in both the serum and liver, with no detectable signs of toxicity including overt behavioral abnormalities, body weight loss, or gross histopathological changes in major organs, indicating acceptable systemic tolerability under the experimental conditions used. Although comprehensive toxicological profiling, including pharmacokinetic analyses and long-term safety assessments, was beyond the scope of the present study, previous reports have

demonstrated favorable systemic tolerability of orally administered adapalene in animal models[48,49]. These observations support the translational potential of adapalene while highlighting the need for future studies to systematically evaluate its pharmacokinetics, dose-dependent toxicity, and long-term safety profile.

In our study, adapalene demonstrated anti-fibrotic effects in both LPS-induced sepsis and HFD-induced obesity mouse models. The anti-fibrotic effects observed in vivo were primarily inferred from reduced hepatic expression of fibrosis-associated markers, including Col1a1 and αSMA, which are well-established indicators of hepatic stellate cell (HSC) activation and fibrogenesis[50]. Although direct assessment of HSC-specific signaling pathways was not performed in vivo, previous studies have demonstrated that retinoid signaling—particularly via RARβ—suppresses HSC activation and extracellular matrix deposition, thereby attenuating liver fibrosis[51–53]. Indeed, we observed that adapalene reduced fibrosis marker expression in LX-2 human hepatic stellate cells in vitro (data not shown). Additionally, activated macrophages are key regulators of HSC activation through the secretion of pro-inflammatory and pro-fibrogenic mediators such as TNFα, IL-1β, and TGF-β[54]. In this study, adapalene robustly suppressed macrophage inflammatory signaling and shifted macrophage polarization away from a pro-inflammatory phenotype, which is known to alleviate paracrine activation of HSCs and promote fibrosis resolution[55,56]. Taken together, these findings suggest that adapalene attenuates hepatic fibrosis through a dual mechanism involving suppression of pro-fibrotic macrophage signaling and potential direct inhibition of HSC activation via retinoid receptor pathways. Future studies employing cell type–specific genetic models or macrophage–HSC co-culture systems will be necessary to definitively delineate the relative contribution of these pathways.

Importantly, the present study extends previous work on retinoids in macrophage biology and metabolic disease in several key aspects. Earlier studies have largely focused on ATRA or broadly acting retinoids and emphasized their general immunomodulatory or metabolic effects without clearly delineating receptor subtype–specific mechanisms[23,57]. In contrast, our findings identify RARβ as a central and functionally dominant retinoid receptor subtype in macrophages, linking retinoid signaling to the coordinated regulation of MAPK, PI3K/Akt, and NF-κB pathways during inflammatory activation, as well as STAT3-dependent M2 polarization. Moreover, while prior studies have typically examined retinoid effects in isolated inflammatory or metabolic contexts, our work demonstrates a unified RARβ-dependent mechanism operating across both acute inflammatory conditions (LPS-induced sepsis) and chronic metabolic disease models (HFD-induced obesity). This integrated approach provides mechanistic insight into how selective retinoid signaling in macrophages can simultaneously modulate inflammation, immune polarization, and metabolic dysfunction, thereby expanding the conceptual framework of retinoid action beyond non-selective or ATRA-centric paradigms.

Conclusion

Although adapalene is currently used externally in clinical settings, its therapeutic potential may be extended to metabolic disorders by targeting adipose and hepatic macrophages. Previously, adapalene has demonstrated systemic efficacy in oral administration studies, particularly in oncology models[49], showing that oral adapalene at doses of up to 100 mg/kg for 3 weeks was effective in cancer model without noticeable toxicity. However, further studies are required to evaluate the chronic toxicity and efficacy of adapalene under systemic exposure to confirm its potential for broader therapeutic applications.

Data availability

The datasets used and analyzed during the current study available from the corresponding author on reasonable request.

Received: 26 October 2025; Accepted: 11 March 2026
Published online: 26 March 2026

References

1. Luo, M., Zhao, F., Cheng, H., Su, M. & Wang, Y. Macrophage polarization: An important role in inflammatory diseases. *Front. Immunol.* **15**, 1352946. https://doi.org/10.3389/fimmu.2024.1352946 (2024).
2. Tugal, D., Liao, X. & Jain, M. K. Transcriptional control of macrophage polarization. *Arterioscler. Thromb. Vasc. Biol.* **33**, 1135–1144. https://doi.org/10.1161/ATVBAHA.113.301453 (2013).
3. Morrissette, N., Gold, E. & Aderem, A. The macrophage-a cell for all seasons. *Trends Cell Biol.* **9**, 199–201. https://doi.org/10.1016/s0962-8924(99)01540-8 (1999).
4. Mantovani, A., Sozzani, S., Locati, M., Allavena, P. & Sica, A. Macrophage polarization: Tumor-associated macrophages as a paradigm for polarized M2 mononuclear phagocytes. *Trends Immunol.* **23**, 549–555. https://doi.org/10.1016/s1471-4906(02)02302-5 (2002).
5. Castoldi, A., Naffah de Souza, C., Camara, N. O. & Moraes-Vieira, P. M. The macrophage switch in obesity development. *Front. Immunol.* **6**, 637. https://doi.org/10.3389/fimmu.2015.00637 (2015).
6. Weisberg, S. P. et al. Obesity is associated with macrophage accumulation in adipose tissue. *J. Clin. Invest.* **112**, 1796–1808. https://doi.org/10.1172/JCI19246 (2003).
7. Li, X. et al. Adipose tissue macrophages as potential targets for obesity and metabolic diseases. *Front. Immunol.* **14**, 1153915. https://doi.org/10.3389/fimmu.2023.1153915 (2023).
8. Lin, S. et al. Targeting parvalbumin promotes M2 macrophage polarization and energy expenditure in mice. *Nat. Commun.* **13**, 3301. https://doi.org/10.1038/s41467-022-30757-y (2022).
9. Zhou, D. et al. Macrophage polarization and function with emphasis on the evolving roles of coordinated regulation of cellular signaling pathways. *Cell. Signal.* **26**, 192–197. https://doi.org/10.1016/j.cellsig.2013.11.004 (2014).
10. Blomhoff, R. & Blomhoff, H. K. Overview of retinoid metabolism and function. *J. Neurobiol.* **66**, 606–630. https://doi.org/10.1002/neu.20242 (2006).
11. Brown, G. The emerging oncogenic role of RARgamma: From stem cell regulation to a potential cancer therapy. *Int. J. Mol. Sci.* **26**, 4357. https://doi.org/10.3390/ijms26094357 (2025).

12. Dolle, P. Developmental expression of retinoic acid receptors (RARs). *Nucl. Recept. Signal.* **7**, e006. https://doi.org/10.1621/nrs.07006 (2009).
13. Duong, V. & Rochette-Egly, C. The molecular physiology of nuclear retinoic acid receptors. From health to disease. *Biochim. Biophys. Acta*. **1812**, 1023–1031. https://doi.org/10.1016/j.bbadis.2010.10.007 (2011).
14. Al Tanoury, Z., Piskunov, A. & Rochette-Egly, C. Vitamin A and retinoid signaling: Genomic and nongenomic effects. *J. Lipid Res.* **54**, 1761–1775. https://doi.org/10.1194/jlr.R030833 (2013).
15. Chiba, T. et al. Retinoic acid signaling coordinates macrophage-dependent injury and repair after AKI. *J. Am. Soc. Nephrol.* **27**, 495–508. https://doi.org/10.1681/ASN.2014111108 (2016).
16. Hong, K. et al. All-trans retinoic acid attenuates experimental colitis through inhibition of NF-kappaB signaling. *Immunol. Lett.* **162**, 34–40. https://doi.org/10.1016/j.imlet.2014.06.011 (2014).
17. Vellozo, N. S. et al. All-trans retinoic acid promotes an M1- to M2-phenotype shift and inhibits macrophage-mediated immunity to *Leishmania major*. *Front. Immunol.* **8**, 1560. https://doi.org/10.3389/fimmu.2017.01560 (2017).
18. Dzhagalov, I., Chambon, P. & He, Y. W. Regulation of CD8 + T lymphocyte effector function and macrophage inflammatory cytokine production by retinoic acid receptor gamma. *J. Immunol.* **178**, 2113–2121. https://doi.org/10.4049/jimmunol.178.4.2113 (2007).
19. Mehta, K., McQueen, T., Tucker, S., Pandita, R. & Aggarwal, B. B. Inhibition by all-trans-retinoic acid of tumor necrosis factor and nitric oxide production by peritoneal macrophages. *J. Leukoc. Biol.* **55**, 336–342. https://doi.org/10.1002/jlb.55.3.336 (1994).
20. Abdelmalek, M. & Spencer, J. Retinoids and wound healing. *Dermatol. Surg.* **32**, 1219–1230. https://doi.org/10.1111/j.1524-4725.2006.32280.x (2006).
21. Shroot, B. & Michel, S. Pharmacology and chemistry of adapalene. *J. Am. Acad. Dermatol.* **36**, S96-103. https://doi.org/10.1016/s0190-9622(97)70050-1 (1997).
22. Lee, N. H. et al. Adapalene induces adipose browning through the RARβ-p38 MAPK-ATF2 pathway. *Arch. Pharm. Res.* **45**, 340–351. https://doi.org/10.1007/s12272-022-01384-4 (2022).
23. Choi, M.J. et al. Anti-obesity effects of Lactiplantibacillus plantarum SKO-001 in high-fat diet-induced obese mice. *Eur. J. Nutr.* **62**, 1611-1622. https://doi.org/10.1007/s00394-023-03096-x (2023).
24. Bastien, J. & Rochette-Egly, C. Nuclear retinoid receptors and the transcription of retinoid-target genes. *Gene* **328**, 1–16. https://doi.org/10.1016/j.gene.2003.12.005 (2004).
25. Kawai, T., Autieri, M. V. & Scalia, R. Adipose tissue inflammation and metabolic dysfunction in obesity. *Am. J. Physiol. Cell Physiol.* **320**, C375–C391. https://doi.org/10.1152/ajpcell.00379.2020 (2021).
26. Fawzy, A. A., Vishwanath, B. S. & Franson, R. C. Inhibition of human non-pancreatic phospholipases A2 by retinoids and flavonoids. Mechanism of action. *Agents Actions* **25**, 394–400. https://doi.org/10.1007/BF01965048 (1988).
27. Kim, B. H., Kang, K. S. & Lee, Y. S. Effect of retinoids on LPS-induced COX-2 expression and COX-2 associated PGE2 release from mouse peritoneal macrophages and TNF-α release from rat peripheral blood mononuclear cells. *Toxicol. Lett.* **150**(2), 191–201. https://doi.org/10.1016/j.toxlet.2004.01.010 (2004).
28. Na, S. Y. et al. Retinoids inhibit interleukin-12 production in macrophages through physical associations of retinoid X receptor and NFkappaB. *J. Biol. Chem.* **274**, 7674–7680. https://doi.org/10.1074/jbc.274.12.7674 (1999).
29. Austenaa, L. M. et al. Vitamin A status significantly alters nuclear factor-kappaB activity assessed by in vivo imaging. *FASEB J.* **18**, 1255–1257. https://doi.org/10.1096/fj.03-1098fje (2004).
30. Purbasari, B. et al. Retinoic acid attenuates nuclear factor kappaB mediated induction of NLRP3 inflammasome. *Pharmacol. Rep.* **74**, 189–203. https://doi.org/10.1007/s43440-021-00321-4 (2022).
31. Reifen, R. et al. Vitamin A deficiency exacerbates inflammation in a rat model of colitis through activation of nuclear factor-kappaB and collagen formation. *J. Nutr.* **132**, 2743–2747. https://doi.org/10.1093/jn/132.9.2743 (2002).
32. Li, S., Lei, Y., Lei, J. & Li, H. All-trans retinoic acid promotes macrophage phagocytosis and decreases inflammation via inhibiting CD14/TLR4 in acute lung injury. *Mol. Med. Rep.* **24**, 868. https://doi.org/10.3892/mmr.2021.12508 (2021).
33. Lo, H. M., Wang, S. W., Chen, C. L., Wu, P. H. & Wu, W. B. Effects of all-trans retinoic acid, retinol, and β-carotene on murine macrophage activity. *Food Funct.* **5**, 140–148. https://doi.org/10.1039/c3fo60309a (2014).
34. Tenorio de Menezes, Y. K. et al. The endogenous retinoic acid receptor pathway is exploited by *Mycobacterium tuberculosis* during infection, both in vitro and in vivo. *J. Immunol.* **211**, 601–611. https://doi.org/10.4049/jimmunol.2200555 (2023).
35. Duester, G. Retinoic acid synthesis and signaling during early organogenesis. *Cell* **134**, 921–931. https://doi.org/10.1016/j.cell.2008.09.002 (2008).
36. Huo, L. et al. All-trans retinoic acid modulates mitogen-activated protein kinase pathway activation in human scleral fibroblasts through retinoic acid receptor beta. *Mol. Vis.* **19**, 1795–1803 (2013).
37. Lin, W. et al. Sulforaphane suppressed LPS-induced inflammation in mouse peritoneal macrophages through Nrf2 dependent pathway. *Biochem. Pharmacol.* **76**, 967–973. https://doi.org/10.1016/j.bcp.2008.07.036 (2008).
38. Bode, J. G., Ehlting, C. & Haussinger, D. The macrophage response towards LPS and its control through the p38(MAPK)-STAT3 axis. *Cell. Signal.* **24**, 1185–1194. https://doi.org/10.1016/j.cellsig.2012.01.018 (2012).
39. Lim, H. J. & Kwak, H. J. Selective PPARδ agonist GW501516 protects against LPS-induced macrophage inflammation and acute liver failure in mice via suppressing inflammatory mediators. *Molecules* **29**, 5189. https://doi.org/10.3390/molecules29215189 (2024).
40. Murray, P. J. & Wynn, T. A. Protective and pathogenic functions of macrophage subsets. *Nat. Rev. Immunol.* **11**, 723–737. https://doi.org/10.1038/nri3073 (2011).
41. Odegaard, J. I. & Chawla, A. Alternative macrophage activation and metabolism. *Annu. Rev. Pathol. Mech. Dis.* **6**, 275–297. https://doi.org/10.1146/annurev-pathol-011110-130138 (2011).
42. Zhuo, Y. et al. Treatment with 3,4-dihydroxyphenylethyl alcohol glycoside ameliorates sepsis-induced ALI in mice by reducing inflammation and regulating M1 polarization. *Biomed. Pharmacother.* **116**, 109012. https://doi.org/10.1016/j.biopha.2019.109012 (2019).
43. Hou, F. F. et al. Macrophage polarization in sepsis: Emerging role and clinical application prospect. *Int. Immunopharmacol.* **144**, 113715. https://doi.org/10.1016/j.intimp.2024.113715 (2025).
44. Yang, Y. H. et al. HNF4A mitigates sepsis-associated lung injury by upregulating NCOR2/GR/STAB1 axis and promoting macrophage polarization towards M2 phenotype. *Cell Death Dis.* **16**, 120. https://doi.org/10.1038/s41419-025-07452-z (2025).
45. Cao, Y. et al. Fenretinide regulates macrophage polarization to protect against experimental colitis induced by dextran sulfate sodium. *Bioengineered* **12**, 151–161. https://doi.org/10.1080/21655979.2020.1859259 (2021).
46. Shoelson, S. E., Herrero, L. & Naaz, A. Obesity, inflammation, and insulin resistance. *Gastroenterology* **132**, 2169–2180. https://doi.org/10.1053/j.gastro.2007.03.059 (2007).
47. Rusu, A. et al. Recent advances regarding the therapeutic potential of adapalene. *Pharmaceuticals (Basel)* **13**, 217. https://doi.org/10.3390/ph13090217 (2020).
48. Shi, X. N. et al. Adapalene inhibits the activity of cyclin-dependent kinase 2 in colorectal carcinoma. *Mol. Med. Rep.* **12**, 6501–6508. https://doi.org/10.3892/mmr.2015.4310 (2015).
49. Friedman, S. L. Hepatic stellate cells: Protean, multifunctional, and enigmatic cells of the liver. *Physiol. Rev.* **88**, 125–172. https://doi.org/10.1152/physrev.00013.2007 (2008).
50. Cortes, E. et al. Retinoic acid receptor-β is downregulated in hepatocellular carcinoma and cirrhosis and its expression inhibits myosin-driven activation and durotaxis in hepatic stellate cells. *Hepatology* **69**, 785–802. https://doi.org/10.1002/hep.30193 (2019).

51. Okuno, M. et al. Increased 9,13-di-cis-retinoic acid in rat hepatic fibrosis: Implication for a potential link between retinoid loss and TGF-β mediated fibrogenesis in vivo. *J. Hepatol.* **30**, 1073–1080. https://doi.org/10.1016/s0168-8278(99)80262-1 (1999).
52. Wang, L. et al. Effects of retinoic acid on the development of liver fibrosis produced by carbon tetrachloride in mice. *Biochim. Biophys. Acta* **1772**, 66–71. https://doi.org/10.1016/j.bbadis.2006.08.009 (2007).
53. Wynn, T. A. & Ramalingam, T. R. Mechanisms of fibrosis: Therapeutic translation for fibrotic disease. *Nat. Med.* **18**, 1028–1040. https://doi.org/10.1038/nm.2807 (2012).
54. Duffied, J. S. et al. Selective depletion of macrophages reveals distinct, opposing roles during liver injury and repair. *J. Clin. Invest.* **115**, 56–65. https://doi.org/10.1172/jci22675 (2005).
55. Krenkel, O. & Tacke, F. Macrophages in nonalcoholic fatty liver disease: A role model of pathogenic immunometabolism. *Semin. Liver Dis.* **37**, 189–197. https://doi.org/10.1055/s-0037-1604480 (2017).
56. Stephensen, C. B. Vitamin A, infection, and immune function. *Annu. Rev. Nutr.* **21**, 167–192. https://doi.org/10.1146/annurev.nutr.21.1.167 (2001).
57. Hall, J. A., Grainger, J. R., Spenced, S. P. & Belkaid, Y. The role of retinoic acid in tolerance and immunity. *Immunity* **35**, 13–22. https://doi.org/10.1016/j.immuni.2011.07.002 (2011).

Author contributions

N.H.L. : Investigation, Methodology, Formal analysis. Data curation. M.J.C.: Investigation, Methodology, Formal analysis. S.M.J. : Software, Data curation. H.J.K. : Conceptualization, Supervision, Funding acquisition, Writing – review & editing. H.G.C. : Conceptualization, Formal analysis, Supervision, Resources. Funding acquisition, Writing – review & editing.

Funding

This research was supported by the Basic Science Research Program through the National Research Foundation of Korea (NRF), funded by the Ministry of Education (Grant No. 2020R1F1A1048327) and the National Research Foundation of Korea (NRF) grant funded by the Korean government (MSIP) (Grant No. NRF-2021R1A2C1012532).

Declarations

Competing interests

The authors declare no competing interests.

Additional information

Supplementary Information The online version contains supplementary material available at https://doi.org/10.1038/s41598-026-44454-z.

Correspondence and requests for materials should be addressed to H.J.K. or H.G.C.